J Appl Electrochem (2012) 42:367–374
DOI 10.1007/s10800-012-0406-4

ORIGINAL PAPER

Synthesis of $Ni(OH)_2$ nanostructures by the hydrothermal treatment in the presence of guanidine carbonate and their electrochemical properties

Go Sakai · Mariko Sugahara

Received: 21 December 2011 / Accepted: 21 March 2012 / Published online: 3 April 2012

Abstract Nanostructure control of β-$Ni(OH)_2$ was attempted by adopting hydrothermal treatment for the high specific surface area (high-SSA) β-$Ni(OH)_2$ in the presence of guanidine carbonate. β-$Ni(OH)_2$ nanosheets-linked structures could be synthesized from high-SSA β-$Ni(OH)_2$ owing to the strong effects of guanidine carbonate for keeping or enlarging SSA during hydrothermal treatment. The discharging capacities of the high-SSA sample showed the highest capacity above 80 % at 0.2*C*. However, the capacities were decreased with decreasing SSA of the β-$Ni(OH)_2$ prepared. It was also found that, at lower SSA, charging/discharging rates below 1*C* did not affect the discharging capacity, i.e., the almost same capacities for 0.2*C* and 1*C*. Cyclic voltammetry revealed that the electrochemical reactions for the charging/discharging were considered to be reversible and smooth at various scanning rates. The rate-determining step of the electrochemical reaction is considered to be regulated by the diffusion of the active species involved for the lower SSA samples. However, for the higher SSA sample ($280\ m^2\ g^{-1}$) obtained at 200 °C in the presence of 1.0×10^{-1} mol L^{-1} guanidine carbonate strongly indicates the effects of the rate of surface reaction or electronic conductivity on rate-determining step of charging/discharging of the material.

Keywords Nickel hydroxide · Hydrothermal treatment · Nanostructures · Electrochemical properties

G. Sakai (✉) · M. Sugahara
Department of Applied Chemistry, Faculty of Engineering, University of Miyazaki, Miyazaki 889-2192, Japan
e-mail: sakai-go@cc.miyazaki-u.ac.jp

1 Introduction

Nickel hydroxide, used as the positive electrode material for Ni-based alkaline batteries, has received considerable attention in nanostructure control to achieve superior electrochemical properties because several literatures have demonstrated the advantages of β-$Ni(OH)_2$ nanostructures in electrochemical properties [1–7]. α-Type $Ni(OH)_2$ nanostructures also have attractive attention because of its unique properties [8, 9]. However, from the practical application point of view, β-$Ni(OH)_2$ is feasible as positive electrode material judging from the stability in strong alkaline media.

The β-$Ni(OH)_2$ has a layered structure in which each layer consists of two sheets of hydroxyls in hexagonal close packing, with a sheet of Ni atoms between them. The layers parallel to the basal plane (001) are weakly stacked by van der Waals forces with an interlayer distance of 0.46 nm. The charging and discharging of β-$Ni(OH)_2$ is considered to take place almost topochemically through insertion and de-insertion of protons in interlayer space. Thus, the rate of charge/discharge process is considered to be determined by proton diffusion, surface exchange reaction, or electronic conductivity of positive electrode [10–15]. However, the contribution of each factor for determining step of charge/discharge process has not been elucidated, although the proton diffusion is considered to be the most important one for charge/discharge processes. Recently, nickel hydroxide particles with a nanostructural multiphase as well as nanometer-sized β-$Ni(OH)_2$ were reported to exhibit superior electrochemical characteristics and higher proton diffusion coefficients [1, 4]. Prompted by the recent progress in nanosciences, we examined here the relationships between β-$Ni(OH)_2$ nanostructures and electrochemical properties to evaluate rate-determining step for

the charge/discharge processes using nanosized β-$Ni(OH)_2$ with high specific surface area (high-SSA).

Our research group have reported that the synthesis of high-specific surface area (high-SSA) β-$Ni(OH)_2$ beyond 200 $m^2\ g^{-1}$ and its transformation into nanosheets and nanodisks by hydrothermal treatment [16]. In the previous study, it was revealed that hydrothermal treatment gave nanosheets at 100–120 °C treatment or nanodisks at 200 °C treatment, respectively. It was also revealed that β-$Ni(OH)_2$ hexagonal plates could be synthesized from the high-SSA β-$Ni(OH)_2$ by the solvothermal treatment using aqueous ammonia solution as the disperse phase [17]. In our previous study, it was indicated that the thickness of the hydrothermally derived β-$Ni(OH)_2$ was strongly influenced by the concentration of coexisting ammonia in water. Thus, the control of nanostructure of β-$Ni(OH)_2$ in the presence of amines was attempted in this study. As the representative amines, ethylenediamine and guanidine carbonate were selected as di-amine and tri-amine, respectively. It was found that the hydrothermal treatment in the presence of guanidine carbonate gave considerable effects on physicochemical properties; however, ethylenediamine hardly gave effects on nanostructures, SSA as well as electrochemical properties. Thus, we report here the effect of guanidine carbonate on β-$Ni(OH)_2$ nanostructures and electrochemical properties of these hydrothermally derived samples.

The hydrothermal treatment of high-SSA β-$Ni(OH)_2$ at elevated temperature up to 200 °C in the presence of guanidine carbonate enlarged the SSA from 235 to 280 $m^2\ g^{-1}$ and the treatment gave sheet-like nanostructures, on contrary to the large decrease in SSA and the formation of hexagonal plates at elevated temperature of 200 °C in the absence of guanidine carbonate or in the presence of ammonia reported in our previous study. For example, as reported elsewhere, hydrothermal treatment at temperature as high as 200 °C led to the formation of β-$Ni(OH)_2$ nanodisks with a low surface area of 39 $m^2\ g^{-1}$.

2 Experimental

All chemicals and solvents used were reagent grade and were used without further purification. High-SSA β-$Ni(OH)_2$ was prepared as the way described in references [16, 17]. Thus, the typical procedure is described briefly as follows. 100 mL of 0.1 M $NiCl_2$ aqueous solution was added dropwise into 1,000 mL of 1 % tetramethylammonium hydroxide (TMAH) aqueous solution at a rate of 1.5 mL min^{-1}, and a pale green suspension was obtained. The obtained suspension was aged for 1 h and filtrated and washed with deionized water successively. The precipitate was collected and dried at 60 °C in air for 0.5 h to obtain high-SSA β-$Ni(OH)_2$. The hydrothermal treatment in the presence of amines was carried out using given amount of ethylenediamine or guanidine carbonate dissolved water as the disperse phase, i.e., 0.2 g of the high-SSA β-$Ni(OH)_2$ was suspended in 20 mL of aqueous solution of ethylenediamine or guanidine carbonate, and the suspensions was transferred into a teflon-lined autoclave (50 mL) and heated at designated temperature (80, 120, or 200 °C) for 12 h. The resulting hydrothermally synthesized hydroxides were collected by filtration and washed with deionized water several times.

XRD patterns were recorded on a Shimadzu XRD-7000 diffractometer using CuKα radiation. N_2 adsorption and desorption isotherms were determined on a Micromeritics Tristar 3000 system at a liquid nitrogen temperature. Before the measurement, the samples were first degassed at 120 °C for 3 h and then under vacuum. The specific surface areas of the samples were calculated with the Brunauer, Emmett, and Teller (BET) method. The mean pore diameters and pore size distributions were determined with the Barrett–Joyner–Halenda (BJH) method using the corresponding desorption branches of the isotherms. Scanning electron microscopy (SEM) images were obtained on a Hitachi S-5500.

Nickel hydroxide electrodes were prepared by incorporating an active paste (0.02 g) into a nickel foam substrate (10 × 10 mm, thickness 0.5 mm), and dried at 120 °C for 10 min. An active paste containing 82 wt% nickel hydroxide samples, 9 wt% commercially available cobalt oxide (Wako Chem., Japan), and 9 wt% carboxymethyl cellulose (CMC) as a binder was prepared by mixing in an agate mortar. The detailed procedure was described in our previous work [16, 17]. Cyclic voltammetry and chronopotentiometry were performed in 6.0 M KOH using the nickel hydroxide electrodes as a working electrode, a rectangular cadmium (Cd) plate as a counter electrode, and Hg/HgO electrode as a reference electrode. The discharge capacity of the nickel hydroxide sample was based on the amount of electrochemically active material (β-$Ni(OH)_2$) excluding cobalt oxide and binder. These electrochemical measurements were carried out using HZ-5000 (Hokuto Denko, Japan) at 25 °C. The charge/discharge rate of C was defined on the basis of the theoretical capacity of β-$Ni(OH)_2$ ($C = 289.15$ mAh g^{-1}).

3 Results and discussion

Figure 1a–c reveals the XRD patterns of the samples obtained by hydrothermal treatment in the presence of guanidine carbonate (concentration: 1.0×10^{-1} mol L^{-1}) at the given temperature of 80, 120, and 200 °C, respectively. All the diffraction peaks were indexed to β-$Ni(OH)_2$

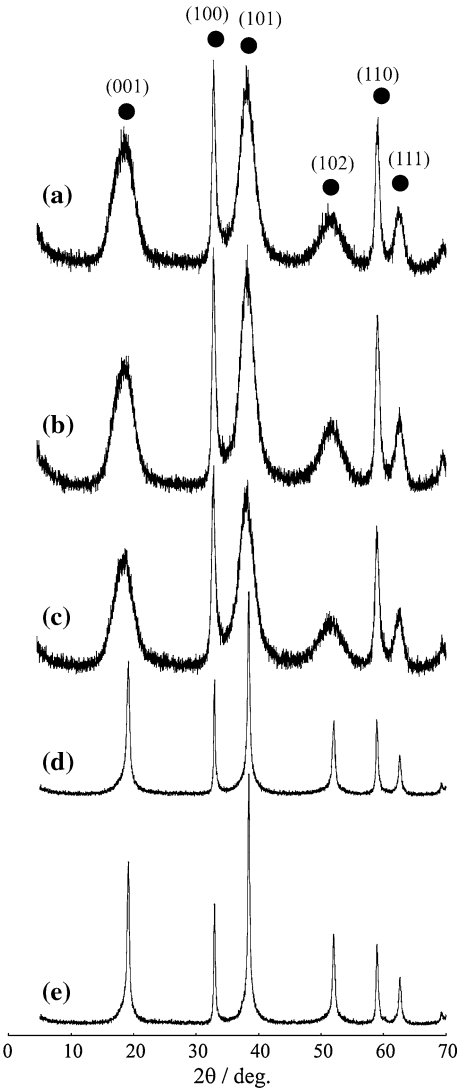

Fig. 1 XRD patterns of the hydrothermally prepared $Ni(OH)_2$ samples under the given conditions of guanidine carbonate concentration and treatment temperature. (*a*) 1.0×10^{-1} mol L^{-1} at 80 °C, (*b*) 1.0×10^{-1} mol L^{-1}at 120 °C, (*c*) 1.0×10^{-1} mol L^{-1} at 200 °C, (*d*) 1.0×10^{-2} mol L^{-1} at 200 °C, and (*e*) 1.0×10^{-3} mol L^{-1} at 200 °C

of a hexagonal structure (PDF No. 14-0117). In the XRD pattern, as reported previously, *c*-axis related peaks of (001), (101), (102), and (111) reflections were very broad, in contrast to the sharp peaks for *c*-axis non-related peaks of (100) and (110) reflections. These XRD peak characteristics are derived from the thinner thickness of *c*-axis and stacking state of nickel hydroxide layers. On the other hand, as shown in Fig. 1d, e, with decreasing the concentration of guanidine carbonate to 1.0×10^{-2} and 1.0×10^{-3} mol L^{-1}, respectively, the *c*-axis related peaks of (001) and (101) became sharp after the hydrothermal treatment at 200 °C. This phenomenon coincide with the hydrothermal treatment in pure water (in the absence of amines), in which *c*-axis related peaks became sharp and resulting in the formation of hexagonal plates. In other words, the presence of guanidine under hydrothermal condition strongly prevents the high-SSA β-$Ni(OH)_2$ from crystal growth in *c*-axis.

Figure 2 shows the SEM photographs of the hydrothermally obtained sample in the presence of guanidine

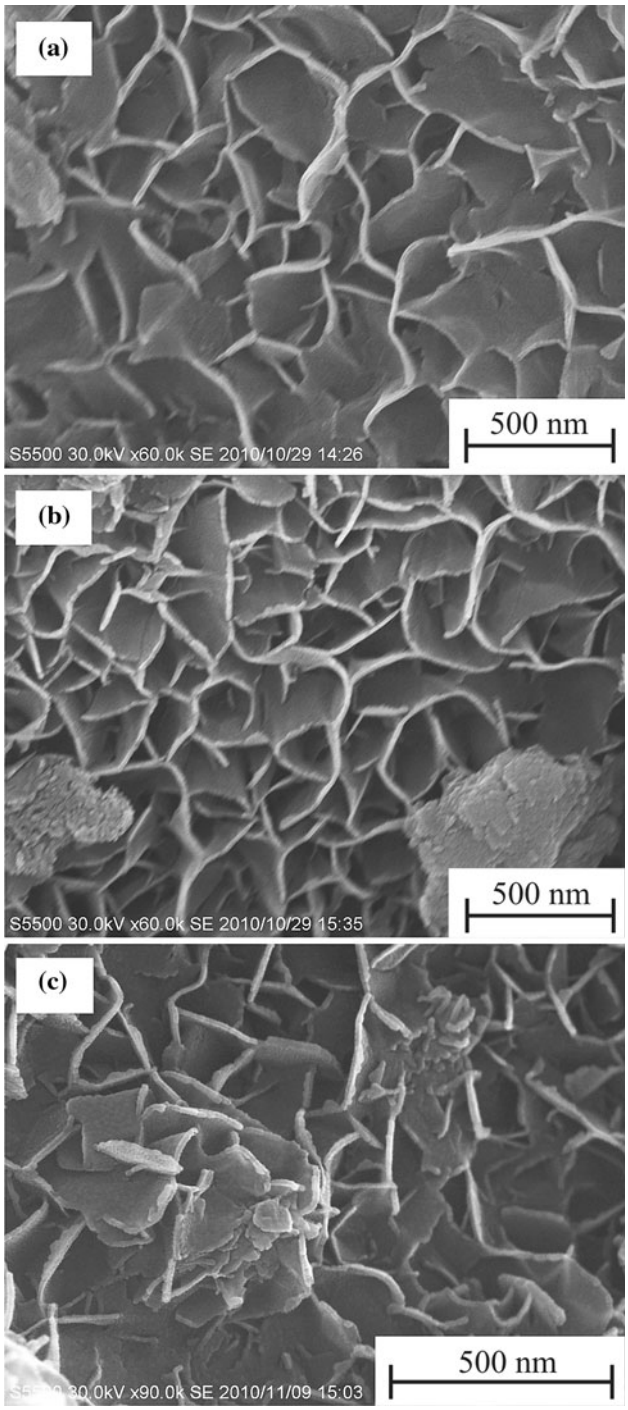

Fig. 2 FE-SEM images of the β-$Ni(OH)_2$ samples obtained by the hydrothermal treatment in the presence of 1.0×10^{-1} mol L^{-1} guanidine carbonate at **a** 80 °C, **b** 120 °C, and **c** 200 °C

carbonate at given temperatures. Similar structures were recognized for these samples, i.e., an aggregate of β-$Ni(OH)_2$ nanosheets. It is seen that nanosheets are linked together to form pores. The nitrogen adsorption–desorption isotherms for the hydrothermally synthesized β-$Ni(OH)_2$ in the presence of guanidine carbonate indicate the similar characteristics and resulting in the similar pore diameter and pore volume, as shown in Fig. 3. These results are summarized in Table 1. As previously reported, it can be speculated that poorly crystallized or amorphous phase contained in the as-precipitated nickel hydroxides could be dissolved hydrothermally in water and re-deposited into well-crystallized hexagonal particles, leading to hexagonal shaped β-$Ni(OH)_2$ nanosheets. Thus, the effects of the guanidine carbonate are considered to enhance the re-deposition of dissolved species onto the facet of hexagonal structure, although the hexagonal structure is rather randomly coagulated in the resulting samples.

Figure 4 shows the hydrothermally obtained samples in the presence of given guanidine carbonate concentration at 200 °C. It is clearly recognized that the β-$Ni(OH)_2$ nanosheets grown in thickness into nanodisks with decreasing the concentration of guanidine carbonate. This result also indicates that the presence of guanidine carbonate under hydrothermal condition have strong effect for preventing high-SSA β-$Ni(OH)_2$ from crystal growth in thickness direction. Table 2 summarized the textural properties of these samples. It can be seen that the hydrothermal

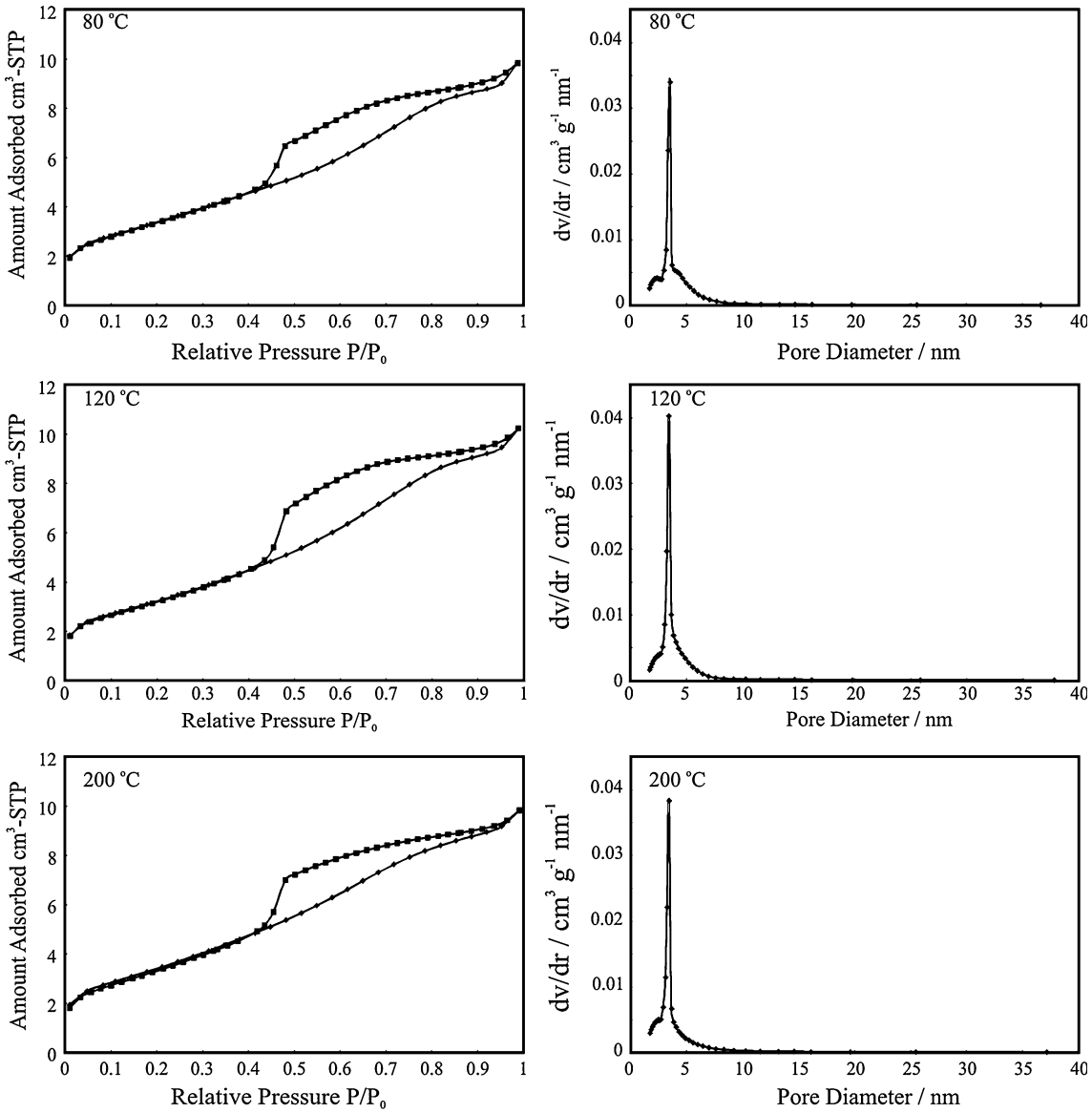

Fig. 3 N_2 adsorption–desorption isotherms and pore size distribution curves obtained from the N_2 desorption isotherms by BJH method for the hydrothermally derived sample in the presence of 1.0×10^{-1} mol L^{-1} guanidine carbonate at given temperatures

Table 1 Specific surface areas, pore volumes, and pore diameters of the β-Ni(OH)$_2$ prepared by the hydrothermal treatment in the presence of 1.0×10^{-1} mol L^{-1} guanidine carbonate at given temperatures

Treatment temperature (°C)	Specific surface area (m^2 g^{-1})	Pore volume (cm^3 g^{-1})	Pore diameter (nm)
Untreated	235	0.14	2.8
80	276	0.32	3.9
120	264	0.34	3.8
200	280	0.32	3.7

treatment in the presence of guanidine carbonate kept high-SSA β-Ni(OH)$_2$ at least 100 m^2 g^{-1} even at high temperature of 200 °C, although the representative pore diameter was slightly enlarged with decreasing guanidine carbonate concentration. The effects of guanidine carbonate during hydrothermal treatment are under investigation; however, this effect would be due to the re-deposition of dissolved species onto the facet of hexagonal structure of β-Ni(OH)$_2$ nanosheets during the hydrothermal treatment. Figure 5 shows the charge/discharge properties of the samples obtained hydrothermally in the presence of given concentration of guanidine carbonate. Each discharge capacities at given *C*-rates is indicated in these figures. As seen from Fig. 5, the discharging capacities of the high-SSA sample derived from hydrothermal treatment in the presence of 1.0×10^{-1} mol L^{-1} guanidine carbonate showed the highest capacity above 80 % at 0.2*C*. However, with decreasing SSA, capacities were decreased in 52 and 45 % for hydrothermally derived samples in the presence of 1.0×10^{-2} and 1.0×10^{-3} mol L^{-1} guanidine carbonate concentrations, respectively. Similarly, the capacities were decreased with decreasing SSA at each *C*-rate indicating that high-SSA is favorable to achieve the higher discharging capacity. On the other hand, at lower SSA (Fig. 5b, c), the capacities at 0.2*C* and 1*C* showed the almost same values indicating that charging/discharging rates below 1*C* do not affect the discharging capacity. Thus, to obtain the higher charging/discharging rates acceptable materials, lower SSA is considered to be an important factor. On the other hand, the shape of the active material, β-Ni(OH)$_2$ nanosheets or nanodisks in the present study, should be considered carefully. Because the β-Ni(OH)$_2$ crystal grown in *c*-axis (thickness direction) hexagonal showed adoptable characteristics as positive electrode material for high charge/discharge rate, as reported previously [17].

Cyclic voltammetry was conducted for the samples derived from hydrothermal treatment. Figure 6 shows the cyclic voltammograms of the hydrothermally derived sample in the presence of 1.0×10^{-1} mol L^{-1} guanidine carbonate at 200 °C, as the typical example. The electrochemical performance of these hydrothermally derived

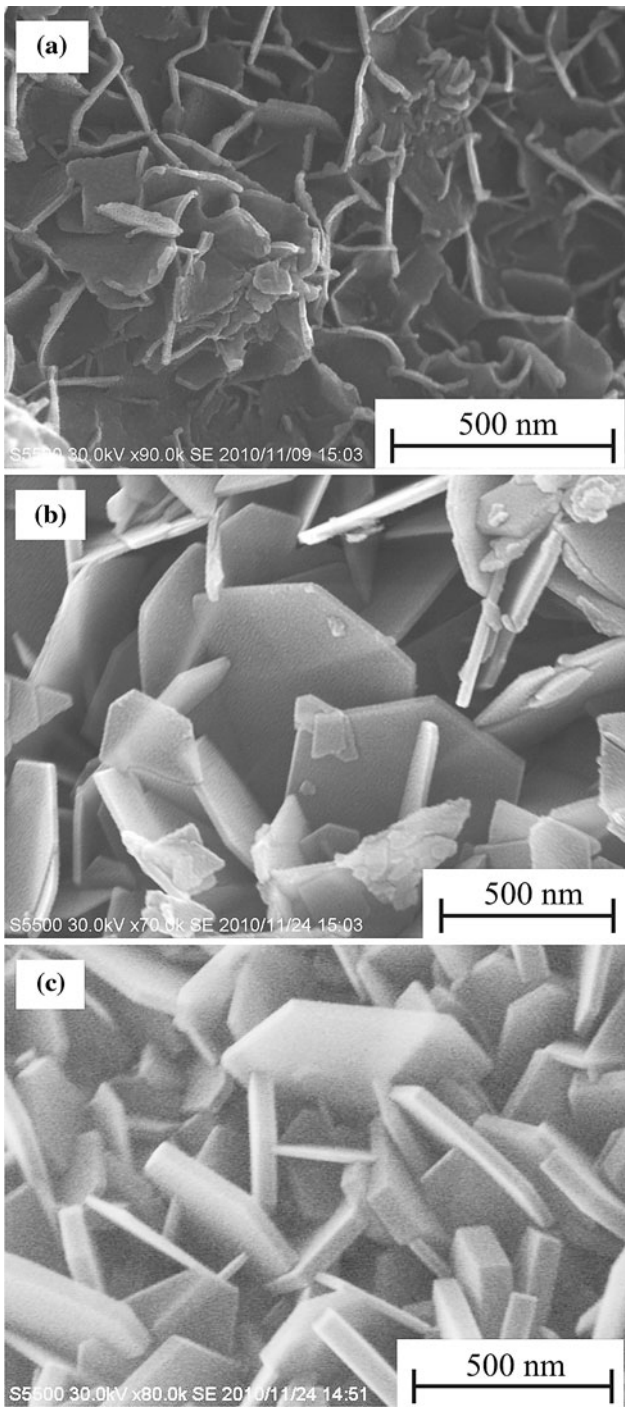

Fig. 4 FE-SEM images of the β-Ni(OH)$_2$ samples obtained by the hydrothermal treatment in the presence of given amount of guanidine carbonate at 200 °C. **a** 1.0×10^{-1} mol L^{-1}, **b** 1.0×10^{-2} mol L^{-1}, and **c** 1.0×10^{-3} mol L^{-1}

β-Ni(OH)$_2$ samples revealed similar reversible and smooth electrochemical reduction–oxidation (redox) processes at various scanning rates. Generally, the peak current, i_p, of reversible electrochemical reaction in cyclic voltammetry will obey the following Eq. (1)

Table 2 Specific surface areas, pore volumes, and pore diameters of the β-Ni(OH)$_2$ prepared by the hydrothermal treatment in the presence of given amount of guanidine carbonate at 200 °C

Guanidine carbonate concentrations (mol L^{-1})	Specific surface area (m^2 g^{-1})	Pore volume (cm^3 g^{-1})	Pore diameter (nm)
1.0×10^{-1}	280	0.32	3.7
1.0×10^{-2}	154	0.30	6.2
1.0×10^{-3}	115	0.27	6.3

$$i_p = 0.4463 \times 10^{-3} n^{3/2} F^{3/2} A (RT)^{-1/2} D^{1/2} C_0 v^{1/2} \quad (1)$$

where n is the electron number of the reaction ($\sim$1 for Ni(OH)$_2$), F is the Faraday's constant, A is the surface area, R is the gas constant, T is the absolute temperature, D is the diffusion coefficient of proton, v is the scanning rate, and C_0 is the initial concentration of the reactant.

When the reaction took place at 25 °C; Eq. (1) is reduced into Eq. (2).

$$i_p = 269 n^{3/2} A D^{1/2} C_0 v^{1/2} \quad (2)$$

When the electrochemical reaction was regulated by the diffusion of the active species involved, the relationships between i_p and $v^{1/2}$ show proportional relationship [1, 18]. Thus, we attempted to plot the anodic peak current, i_{pa}, and cathodic peak current, i_{pc}, with respect to square root of the scanning rate, $v^{1/2}$. However, as shown in Fig. 6, the anodic peak current (oxidation peaks), i_{pa}, was difficult to recognize. It can be seen that the shoulders at about 0.47 V (vs. Hg/HgO). The chronopotentiometric results, charge/discharge characteristics shown in Fig. 5, also showed the charging potential reaches plateau at about 0.47 V (vs. Hg/HgO). Thus, the anodic peak currents (oxidation peaks), i_{pa}, were determined at 0.47 V (vs. Hg/HgO). The cathodic peak current, i_{pc}, was relatively well recognized and obtained at 0.29 V (vs. Hg/HgO). As shown in Fig. 7, the lower SSAs samples showed almost proportional relationships between i_p and $v^{1/2}$ (Fig. 7b, c) indicating that the rate-determining step of the electrochemical reaction is regulated by the diffusion of the active species involved. The charging and discharging of β-Ni(OH)$_2$ is considered to take place almost topochemically through insertion and de-insertion of protons in interlayer space. Generally, it is believed that the diffusion of proton is the rate-determining step for the β-Ni(OH)$_2$ positive electrode material. Actually, the results shown in Fig. 7b, c indicate the diffusion controlled characteristics. The almost same slopes between oxidation and reduction for each samples indicate the electrochemical reaction is controlled by same chemical process for charging and discharging. Thus, the reaction may be controlled by one chemical species, i.e., proton (H^+). On contrary, the high-SSA sample obtained at

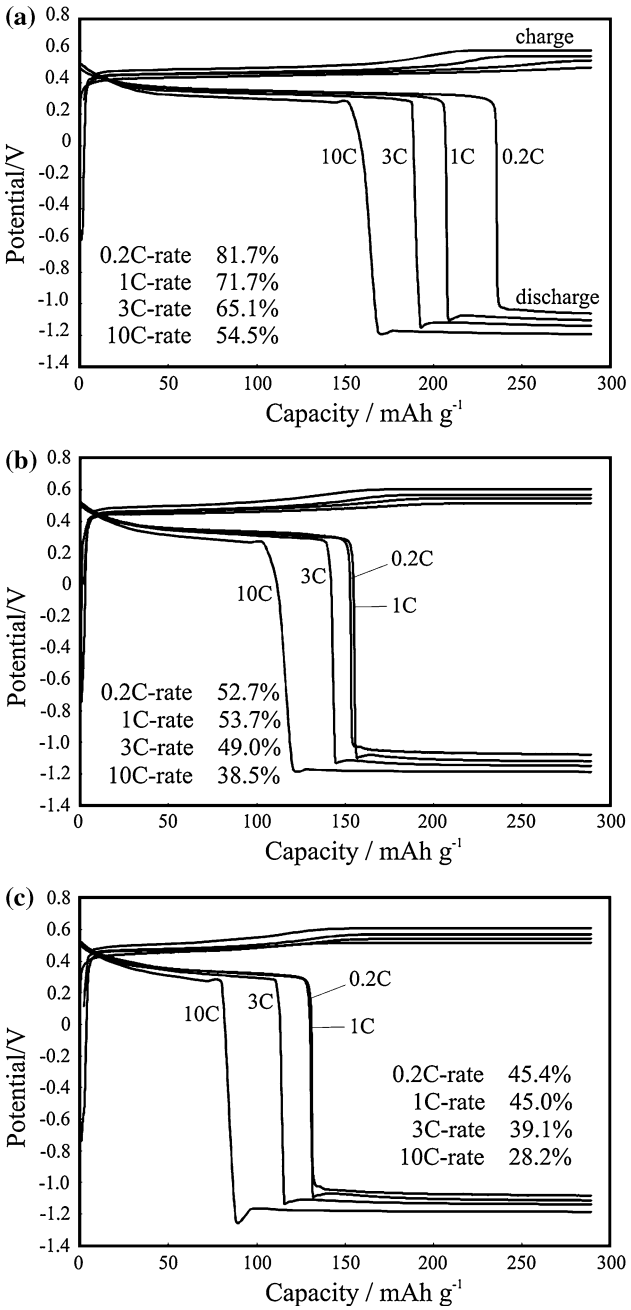

Fig. 5 Charge/discharge curves for three kinds of hydrothermally derived β-Ni(OH)$_2$ samples obtained at given amount of guanidine carbonate at 200 °C (**a** 1.0×10^{-1} mol L^{-1}, **b** 1.0×10^{-2} mol L^{-1}, and **c** 1.0×10^{-3} mol L^{-1}). The discharging capacities at each charge/discharge rates are indicated in the figures

200 °C in the presence of 1.0×10^{-1} mol L^{-1} guanidine carbonate does not show linear relationships between i_p and $v^{1/2}$, for both anodic and cathodic reactions, as shown in Fig. 7a, indicating that the rate-determining step is controlled not only by the diffusion of the active species involved but also by the rate of surface reaction involved or

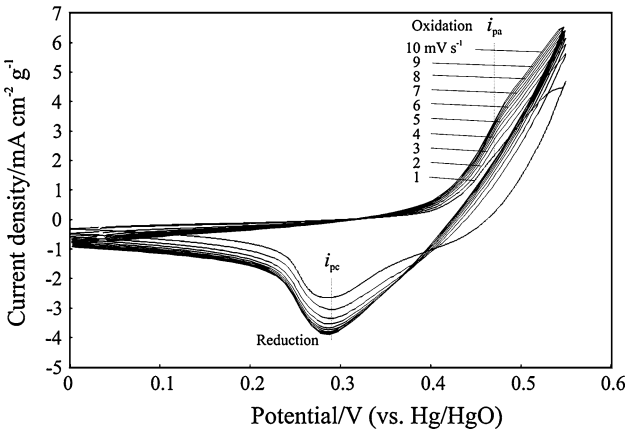

Fig. 6 Cyclic voltammograms obtained at various scanning rates for the hydrothermally derived β-Ni(OH)$_2$ sample in the presence of 1.0×10^{-1} mol L^{-1} guanidine carbonate at 200 °C

electronic conductivity of the material. The electronic conductivity was considered to be almost same level for the hydrothermally derived samples so that the electrochemical surface reaction of charge/discharge was considered to be the rate-determining step for the high-SSA sample obtained at 200 °C. Further study is needed to elucidate the contribution of the rate of surface reaction to rate-determining step and competition between diffusion and reaction of the active species. The present study strongly indicates that the contribution of the rate of surface reaction cannot be neglected when increasing the specific surface area of active materials, although the critical level of the specific surface area will depend on the rate of surface electrochemical reaction.

4 Conclusions

It was found that the β-Ni(OH)$_2$ nanostructure, i.e., nanosheets-linked structure could be synthesized from high-SSA β-Ni(OH)$_2$ under hydrothermal condition in the presence of guanidine carbonate. The presence of guanidine carbonate showed the strong effect to keeping or enlarging of SSA in resulting product of β-Ni(OH)$_2$, i.e., the 280 m^2 g^{-1} (1.0×10^{-1} mol L^{-1}), 154 m^2 g^{-1} (1.0×10^{-2} mol L^{-1}), and 115 m^2 g^{-1} (1.0×10^{-3} mol L^{-1}) even at 200 °C treatment. The discharging capacities of the high-SSA sample showed the highest capacity above 80 % at 0.2*C*. However, the capacities were decreased with decreasing SSA at each *C*-rate indicating that high-SSA is favorable to achieve the higher discharging capacity. On the other hand, at lower SSA, charging/discharging rates below 1*C* do not affect the discharging capacity. Cyclic voltammetry revealed reversible and smooth electrochemical reduction–oxidation (redox) processes at

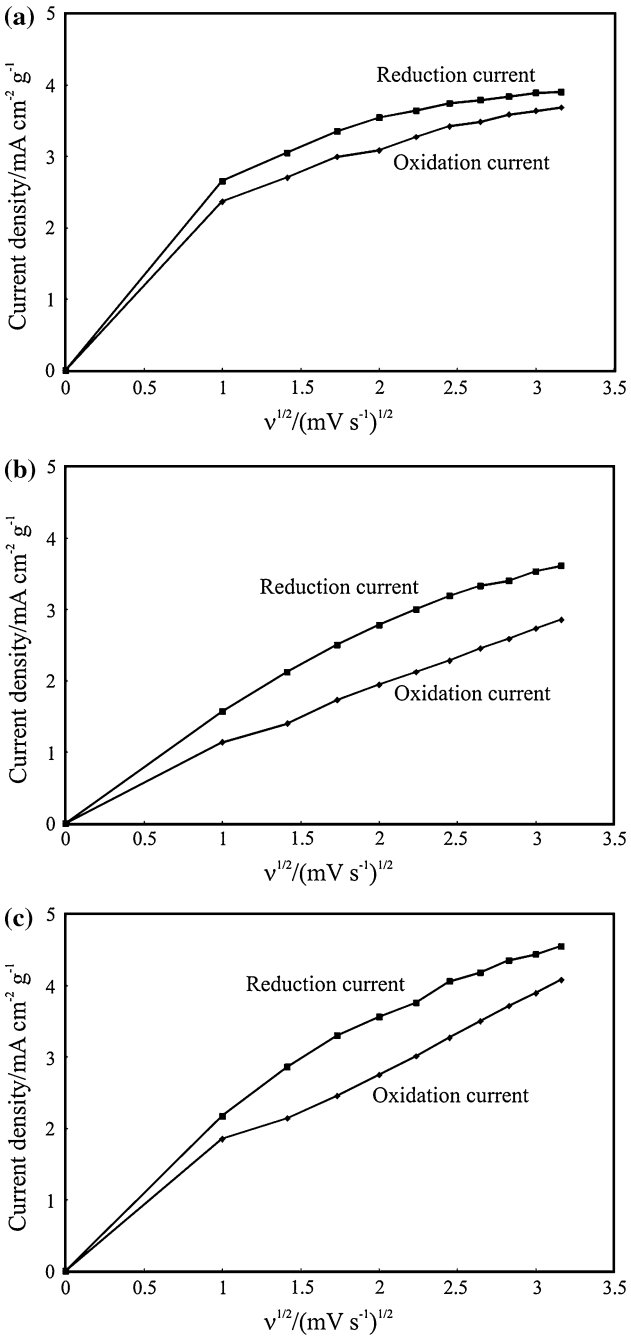

Fig. 7 Relationships between i_p and $v^{1/2}$ for the hydrothermally derived β-Ni(OH)$_2$ samples in the presence of given amount of guanidine carbonate at 200 °C. (Guanidine carbonate concentration; **a** 1.0×10^{-1} mol L^{-1}, **b** 1.0×10^{-2} mol L^{-1}, and **c** 1.0×10^{-3} mol L^{-1})

various scanning rates. The relationships between the peak current and square root of the scanning rate showed that the rate-determining step of the electrochemical reaction is regulated by the diffusion of the active species involved for the lower SSA samples. On contrary, the high-SSA sample obtained at 200 °C in the presence of 1.0×10^{-1} mol L^{-1}

guanidine carbonate implied the effects of the rate of surface reaction or electronic conductivity of the material on rate-determining step of charge/discharge processes.

References

1. Han XJ, Xu P, Xu CQ, Zhao L, Mo ZB, Liu T (2005) Electrochim Acta 50:2763
2. Yang D, Wang R, He M, Zhang J, Liu Z (2005) J Phys Chem B 109:7654
3. Song QS, Li YY, Chan SLI (2005) J Appl Electrochem 35:157
4. Wang X, Luo H, Parkhutik PV, Millan A, Matveeva E (2003) J Power Sources 115:153
5. Liu X, Yu L (2004) Mater Lett 58:1327
6. Chen D, Gao L (2005) Chem Phys Lett 405:159
7. Cai F, Zhang G, Chen J, Gou X, Liu H, Dou S (2004) Angew Chem Int Ed 43:4212
8. Xu L, Ding Y, Chen C, Zhao L, Rimkus C, Joesten R, Suib SL (2008) Chem Mater 20:308
9. Cao M, He X, Chen J, Hu C (2007) Cryst Growth Des 7:170
10. Oshitani M, Yufu H, Takashima K, Tsuji S, Matsumaru Y (1989) J Electrochem Soc 136:1590
11. Delmas C, Braconnier JJ, Borthomieu Y, Hagenmuller P (1987) Mater Res Bull 22:741
12. Guerlou-Demourgues L, Denage C, Delmas C (1994) J Power Sources 52:269
13. Akinc M, Jongen N, Lemaitre J, Hofmann H, Euro J (1998) Ceram Soc 18:1559
14. Hu W, Gao X, Noreus D, Burchardt T, Nakstad NK (2006) J Power Sources 160:704
15. Delahaye-vidal A, Figlarz M (1987) J Appl Electrochem 17:589
16. Sakai G, Miyazaki M, Kijima T (2010) J Electrochem Soc 157:A480
17. Sakai G, Miyazaki M, Kijima T (2010) J Electrochem Soc 157:A932
18. Cao X, Wei J, Luo Y, Zhou Z, Zhang Y (2000) Int J Hydrogen Energy 25:643